IEEE Access
Multidisciplinary ⋮ Rapid Review ⋮ Open Access Journal

Received 11 February 2023, accepted 25 February 2023, date of publication 6 March 2023, date of current version 10 March 2023.

*Digital Object Identifier 10.1109/ACCESS.2023.3252913*

RESEARCH ARTICLE

# Hexagonal-Triangular Combinatorial Structure Based Dual-Band Circularly Polarized Patch Antenna for GAGAN Receivers

**C. SAHANA, (Graduate Student Member, IEEE), M. NIRMALA DEVI, (Member, IEEE), AND M. JAYAKUMAR, (Member, IEEE)**

Department of Electronics and Communication Engineering, Amrita School of Engineering, Amrita Vishwa Vidyapeetham, Coimbatore 641112, India

Corresponding author: M. Nirmala Devi (m_nirmala@cb.amrita.edu)

**ABSTRACT** A multilayer gap-coupled dual-band hexagonal microstrip patch antenna is presented for GPS Aided GEO Augmented Navigation (GAGAN) receivers. GAGAN is developed by AAI (Airport Authority of India) and ISRO (Indian Space Research Organization) exclusively for aviation purposes, with GPS frequencies of L5 (1176.45 MHz) and L1 (1575.42 MHz). The proposed GAGAN antenna has three trapezoidal and four equilateral triangular patch resonators configured to form a gap-coupled hexagonal patch on the top layer and seven equilateral triangular patches with slots in between to form the middle layer. Both layers are fed by a single coax feed to achieve a dual-band compact microstrip antenna with dimensions of 55 mm x 55 mm x 3.2 mm. Instead of designing the hexagonal antenna conventionally from a circular patch antenna, the sides of the equilateral triangular patch are truncated to obtain the proposed compact hexagonal antenna, as the triangular antenna occupies less area than circular or square patches for a fixed frequency. To bring novelty with improved performance, the combinatorial structured configuration is explored through step-by-step optimization. GAGAN requirements, such as circular polarization with a single input, dual-band operation, and high gain with gain flatness, are achieved with this compact structured antenna when compared to square and circular patch antennas. Combinatorial structures, such as perturbation and truncation, introduced in the patches are responsible for exciting two near-degenerate orthogonal modes that produce circular polarization (CP). A cross-slot etched in the center patch results in gain enhancement with a gain above 3.2 dBi over a bandwidth of 20 MHz in both bands. Five shorting pins are added to achieve high impedance matching and good CP, with an axial ratio (AR) of less than 2 dB. The simulated and measured results are found to be in good agreement with greater than 20 MHz operational bandwidth exhibiting CP with an omni-directional radiation pattern having high cross-polar levels of -22 dB. The size reduction achieved in the proposed design is 56.79% compared with the conventional hexagonal patch antenna. The measured 10 dB impedance bandwidth is 2.7% and 2.1% for L5 and L1 bands respectively with a 3 dB AR bandwidth of 2.3% for L5 and 2.0% for L1, satisfying the GAGAN requirements.

**INDEX TERMS** Circular polarization, dual-band, global positioning system (GPS), GPS aided GEO augmented navigation receivers (GAGAN), hexagonal antenna, multilayer, triangular antenna.

## I. INTRODUCTION

GPS Aided GEO Augmented Navigation (GAGAN) is an Indian Satellite Based Augmentation System (SBAS), that redefines navigation over Indian Airspace. The use of satellite-based navigation in the civil aviation sector has increased to enhance the efficiency, safety, and reliability of civilian aircraft flying over Indian skies and adjoining areas [1]. The SBAS is a wide-area augmentation system that provides augmented accuracy and integrity to navigation signals such as GPS. Fig. 1 shows the elements present in GAGAN along with its working principle [2]. The

The associate editor coordinating the review of this manuscript and approving it for publication was Tutku Karacolak.

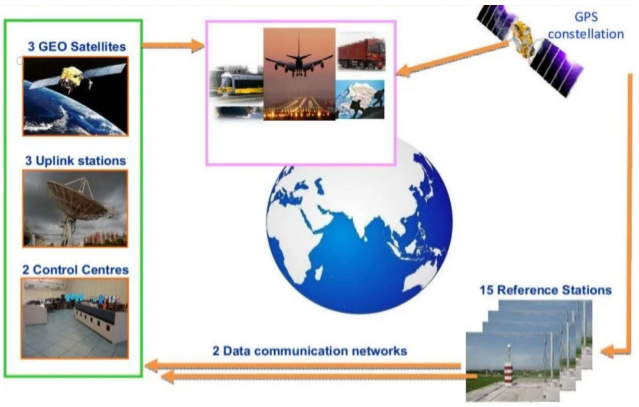


**FIGURE 1.** Description of GAGAN and its applications [2].

GAGAN system comprises three GEO satellites (GSAT 8, GSAT 10, and GSAT 15) and GPS satellites in the space segment. In the ground segment, there are 15 Indian Reference Stations (INRES), 2 Indian Master Control Centre (INMCC) and 3 Indian Navigation Land Uplink Station (INLUS). The INRES stations positioned across various locations collect data from all GPS and GEO satellites and forward them to the INMCC, where the GPS information is processed to generate SBAS messages. The SBAS message contains information that allows the SBAS receiver to remove the errors. The generated SBAS messages are sent to INLUS and hence uplinked to Geo satellites from where the messages are broadcasted to the user community. Any SBAS-enabled receiver can receive this signal to remove errors in the GPS position solution, thus increasing location accuracy, connectivity and integrity. GAGAN's potential extends beyond aviation to military, forest management, marine and freight management, Indian highways, railways, surveying, unmanned aerial vehicle (UAE) such as drones, and for personal users of position location applications. GAGAN receivers operate at frequencies L5 (1176.45 MHz) and L1 (1575.42 MHz) of 20 MHz bandwidth to reduce the pseudo-range error and hence improve the location accuracy.

The primary requirement of a GAGAN operating in the L-band is the design of a low-profile circularly polarized antenna that calls for a microstrip patch antenna [3], [4], [5], [6]. Compared to other patch antennas, triangular antennas occupy less area, resulting in a compact structure [7]. By etching a V-shaped slot on an equilateral triangular patch with a truncated tip [8], a dual-band response is produced, where the size is reduced to half by introducing two shorting walls. The triangular patch slotted antenna in [9] has three triangular slots, resulting in a multiband operation with a gain greater than 10 dBi in all bands. A wideband equilateral triangular patch with a differential feed and a side length of 6.5 mm [10] produces a wide impedance bandwidth of 50.46% by introducing shorting pins. The outcome of various slot shapes on a triangular patch for compactness is studied in [11], where the size reduction achieved using triangular slots is approximately 18.86%. Further size reduction is achieved by incorporating a multilayer antenna structure [12], involving two pentagon rings evolved by truncating an equilateral triangular ring antenna producing CP with a size reduction of 54%. By introducing circuitry elements into annular patch rings [13], [14], CP is produced with dual-band operation with reduced cross-polarization radiation levels. Similarly, through a pair of slits and a quarter-wavelength arc, CP is produced in [15]. Although it is a single-fed ring antenna, its size is larger for specified applications. In [16], a single coax-fed rectangular patch antenna has a complex structure with four different slots introduced in the four quadrants of the patch to excite two degenerate orthogonal modes generating CP with a narrow 3 dB axial ratio bandwidth and low gain. Because the impedance bandwidth (IBW) and axial ratio bandwidth (ARBW) are lower in [12], [13], [14], [15], and [16], many techniques for improving the bandwidth with circular polarization have been discussed in [5], [17], [19], [20], [21], [22], and [23], involving various hexagonal structures [5], [19], [20], [21], [22]. Simple stacked circular patches with CP dual-band operation [17] have an annular metal strip loaded with a ground plane with edge resistors to enhance the ARBW (9.6% and 7.1%) and a coupled-line transdirectional coupler to generate CP. The main disadvantage is that the feed structure is very complex, which makes it difficult to fabricate. By tuning the gap introduced between the hexagonal loops [5], CP is produced with a wide IBW of 14.7% and ARBW of 6.2% with a relatively low gain of 2.4 dBi. A miniaturized split-ring hexagonal resonator with a size of 20 mm $\times$ 20 mm [19] produces multiband resonance upon the introduction of each ring to produce a 15.8% IBW. Although it is compact, the gain is less than 0.5 dBi due to the smaller ground plane. The gain is improved in [20] by incorporating a sequentially rotated hexagonal patch array on a larger substrate, resulting in a gain of greater than 5 dBi with a wide IBW. Although the single antenna is omnidirectional, the hexagonal array exhibits a narrow radiation pattern owing to its thicker substrate. A CP hexagonal slot antenna with a broadband L-shaped monopole patch [21], produces an IBW of 86% and an ARBW of 50% by introducing perturbations around the slots. Because the monopole is not a symmetrical structure, radiation is not omnidirectional. The hexagonal antennas discussed above are either linearly or circularly polarized with no broadside radiation and have complex feed structures, making them difficult to fabricate. Thus, a compact antenna that is circularly polarized with an omnidirectional pattern satisfying GAGAN requirements is necessary. A multilayer, dual-band CP hexagonal antenna with GAGAN specifications is proposed in this work, where the structure resembles a hexagonal antenna [22] in certain ways, with linear polarization adopted for different objectives and operational frequencies.

In this study, a multilayer gap-coupled dual-band hexagonal microstrip patch antenna is presented. It has three trapezoidal and four equilateral triangular patch resonators arranged to form a gap-coupled hexagonal patch on the top

layer and seven equilateral triangular patches with slots in between at the middle layer for multiband operation. The hexagonal antenna is conventionally derived from a circular patch antenna in most of the reported works, where the size is relatively large for the L-band. However, the proposed work targets compactness; hence, the structure is derived from an equilateral triangular antenna with truncation, as it occupies less area than circular or square patches for a fixed frequency. The size reduction achieved in the proposed design is 56.79% compared to the conventional hexagonal patch antenna. Aspects of GAGAN requirements, such as circular polarization with a single input, dual-band operation, and high gain with gain flatness, are achieved with this compact structured antenna through combinatorial configurations. This combinatorial antenna, fed by a coax feed, has fewer antenna elements to achieve a compact microstrip antenna. The size and technical performance of the antenna were improved by adopting this configuration, where different geometric shapes and configurations of the patch element were implemented to optimize the performance of the antenna. As the objectives of GAGAN are contradictory, step-by-step evolution and optimization have been performed through structural modifications to obtain the required objectives. Because the proposed work targets the GAGAN application, the antenna is designed for frequencies L5 and L1. The antenna design, its structural evolution, parametric analysis, and fabricated and measured results are subsequently discussed in detail.

## II. ANTENNA DESIGN AND ANALYSIS

### A. ANTENNA GEOMETRY

The proposed unconventional hexagonal patch antenna in Fig. 2, has seven patch resonators in the top layer, with four equilateral triangular patches and three trapezoidal patches that are repeated to form a hexagonal patch antenna. The center patch is excited by a 50 Ω coax feed, as shown in Fig. 2(a), which excites all the other resonators through gap coupling. The middle layer in Fig. 2(b) consists of seven equilateral triangular patches with slots between them to produce a multiband operation. The top and middle patches are printed on a Roger RT/Duroid 6002 substrate with a thickness of 1.6 mm, relative permittivity $\varepsilon_r = 2.94$ and $tan\delta = 0.0012$. The total size of the antenna including the ground plane is 55 mm × 55 mm. The top and middle layers produce resonance at 1176.45 MHz (L5) and 1575.42 MHz (L1), respectively. Middle triangular patches are constructed to maintain the geometrical symmetry of the upper hexagonal patch. To maintain compactness, a coupling gap $d$ of 0.2 mm is fixed between the patches in the top layer to produce three trapezoidal and four triangular patch resonators. Impedance matching can be improved by reducing the reflected power by optimizing the size of the coupling gap $d$. A conventional hexagonal patch antenna is derived from a circular patch antenna with the same radius. An empirical formula [24] that can be used to calculate the dimensions of a hexagonal patch

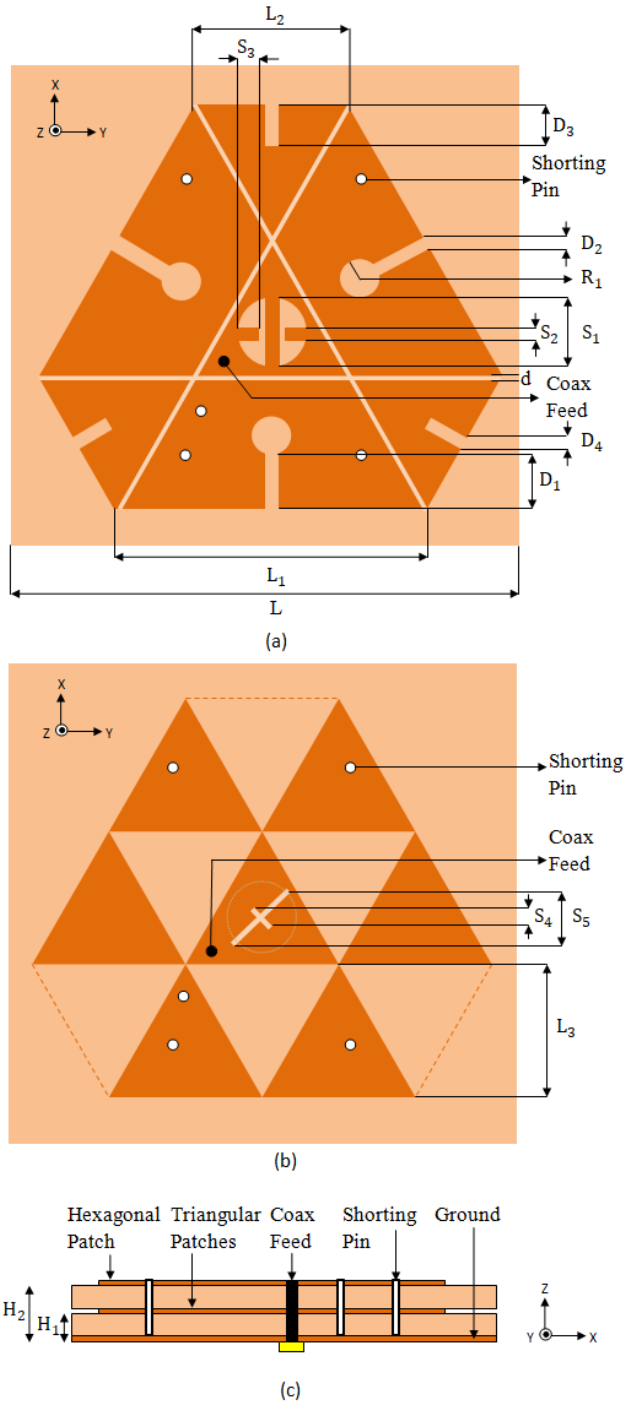


**FIGURE 2.** Proposed antenna (a) Top view-top layer (b) Top view-middle layer (c) Side view.

antenna is given by equation (1).

$$f_o = \frac{c}{2\pi a\sqrt{\frac{\varepsilon_r + 1}{2}}} \tag{1}$$

where, $f_o$ - resonant frequency of the antenna
$c$ - speed of light
$\varepsilon_r$ - relative dielectric constant of the substrate
$a$ - radius of the hexagonal patch (40.32 mm).

This formula is an approximation and the actual resonant frequency of a hexagonal patch antenna can vary depending on various factors such as the dielectric constant of the substrate, the feed location and the shape of the patch. Triangular patch antennas are often used in microstrip antennas because they occupy less area than circular or square patches for a fixed frequency with good radiation performance. Among these, equilateral triangular patch antennas are very common because of their small size and low cost. Hence, this triangular patch is used as the basic structure for the proposed hexagonal patch evolution to obtain compactness that satisfies the GAGAN requirements. The proposed hexagonal antenna is obtained by truncating the sides of a conventional equilateral triangular patch [24], whose resonant frequency is given by equation (2).

$$f_r = \frac{cK_{mn}}{2\pi\sqrt{\varepsilon_r}} = \frac{2c\sqrt{m^2+mn+n^2}}{3b\sqrt{\varepsilon_r}} \tag{2}$$

where, $b$ - side length of the equilateral triangular antenna
$K_{mn}$ - the wave number given in equation (3)
$c$ - the velocity of light
$\varepsilon_r$ - dielectric constant
$mn$ - $TM_{mn}$ mode with m=1, n=0

$$K_{mn} = \frac{4\pi\sqrt{m^2+mn+n^2}}{3b} \tag{3}$$

The expression for lowest order resonant frequency is

$$f_r = \frac{2c}{3b\sqrt{\varepsilon_r}} \tag{4}$$

In this relation, the effect of the fringing fields is not considered. Because the electrical length is larger than the physical length owing to the fringing fields, $\varepsilon_r$ and $b$ are replaced by the effective dielectric constant, $\varepsilon_{eff}$ and modified side length, $b_{eff}$ as given in equations (5-7).

$$\varepsilon_{eff} = \frac{1}{2}(\varepsilon_r+1) + \frac{1}{4}\frac{(\varepsilon_r-1)}{\sqrt{1+\frac{12h}{b}}} \tag{5}$$

$$b_{eff} = b + \frac{h}{\varepsilon_r} \tag{6}$$

$$f_r = \frac{2c}{3b_{eff}\sqrt{\varepsilon_{eff}}} \tag{7}$$

Thus, equation (7) gives the resonant frequency, including the effect of the fringing field. The values obtained for the above equations when operated at L5 (1.176 GHz) are $b$ = 99.27 mm; $b_{eff}$ = 100.8 mm; $\varepsilon_{eff}$ = 2.85. By incorporating a multilayer structure, the final length of the hexagonal patch is 35 mm. A size reduction of approximately 56.79% is achieved using a triangular patch when compared to the conventional circular patch antenna for designing a hexagonal antenna. Combinatorial configurations (such as perturbation and truncation) are powerful tools in the design of patch antennas because they allow for efficient exploration of the design space to find the optimal configuration for a given set of design constraints. These combinatorial optimization techniques involve systematically evaluating different combinations of geometric parameters, such as the shape, size, and position of the patch; the size and shape of the ground plane; and the position of the feed. By testing different configurations, the combination that provides the best performance can be identified. Thus, three rectangular and dumbbell slits excite the fundamental mode of the patch [25], lowering the resonant frequency for circular polarization (CP) at L1. By tuning the distance between the perpendicular stubs in the center, good CP performance is produced at L5. Thus, by optimizing the length of the perturbations and stubs, two orthogonal near-degenerate modes are excited to produce CP with high cross-polar radiation levels. Because the coupling between two layers alters antenna performance, the evolution also considers this coupling effect. The design parameters are optimized using HFSS to achieve good performance, as presented in Table 1.

**TABLE 1. Optimized parameters.**

| Parameter | $L$ | $L_1$ | $L_2$ | $L_3$ | $D_1$ | $D_2$ | $D_3$ | $D_4$ |
|---|---|---|---|---|---|---|---|---|
| Value(mm) | 50 | 24 | 12 | 12 | 4.59 | 1 | 3 | 1 |
| Parameter | $S_1$ | $S_2$ | $S_3$ | $S_4$ | $S_5$ | $R_1$ | $H_1$ | $H_2$ |
| Value(mm) | 5.91 | 1 | 1.46 | 2.2 | 6 | 1.5 | 1.6 | 3.2 |

### B. STRUCTURAL EVOLUTION

The structural evolution of the top and middle layers of the proposed antenna are shown in Figs. 3 and 4, respectively. The corresponding reflection coefficient and axial ratio (AR) plots are shown in Figs. 5 and 6, respectively. Table 2 shows the performance comparison during the structural evolution in terms of size, reflection coefficient, AR, and gain. The design begins with a conventional equilateral triangular patch antenna, as shown in Fig. 3(a), fed by a single coax feed, producing a single resonance at L5. For simplicity, coaxial feeding is used because the coaxial cable impedance, in general, is 50 Ω. There are a large number of points inside the patch with 50 Ω impedance. These points constitute a locus known as the 50 Ω locus. Feeding at any of these points results in maximum radiation because of the perfect matching. Through optimization, the patch is fed at an optimum feed location $(x_o, y_o)$ (along the 50 Ω locus), as shown in Figure 3(a), using a coax feed. The three corners of this antenna are truncated, resulting in a hexagonal antenna, as shown in Fig. 3(b). On truncating the sides, AR starts to decrease with resonance at L5. By adjusting the length of the truncated tip, the fundamental resonant mode gets split into two near-degenerate orthogonal modes for the CP radiation. Because the top layer has only one resonance at L5, a layer consisting of seven equilateral triangular patches, as shown in Fig. 4(a), is introduced below the hexagonal antenna in Fig. 3(b) to produce dual resonance around L5 and L1. Three rectangular slits and dumbbell-shaped slots were introduced on the triangular and trapezoidal patches respectively as shown in Fig. 3(c), to produce circular polarization (CP) in L5. As the AR is greater than 3 dB between 1.4 to 1.6 GHz, CP is generated around L1 by

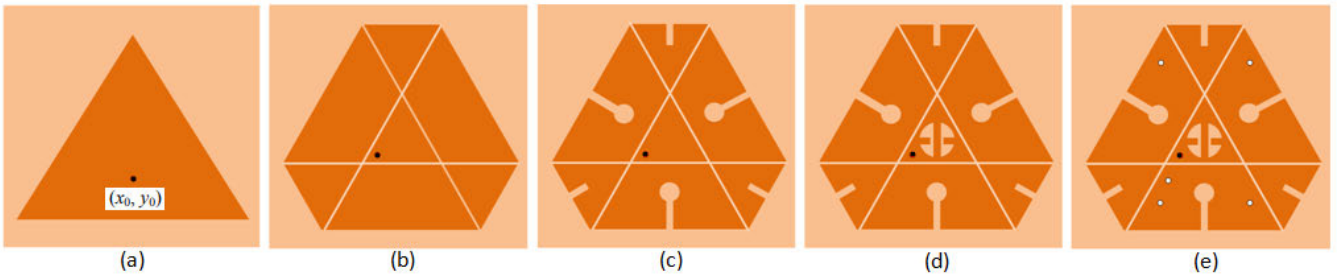


**FIGURE 3.** Structural evolution - Top Layer.

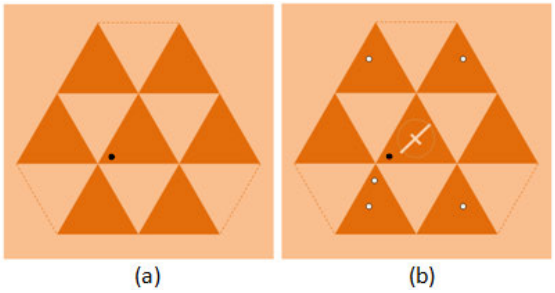


**FIGURE 4.** Structural evolution - Middle Layer.

incorporating two perpendicular stubs in the center triangular patch as shown in Fig. 3(d). To obtain a high impedance matching and good CP, five shorting pins are added as shown in Figs. 3(e) and 4(b). The shorting pins perturb the field distribution beneath the patch because of the shunt inductance effect. The shorting pin present below the coax feed is added to tune the axial ratio to be less than 3 dB at L1. By adjusting the position of the shorting pins, the influence on field distribution gets strengthened to achieve its dominant mode, thus producing circular polarization. A cross slot is etched in the center patch of the middle layer for gain enhancement throughout the two operating bands with a bandwidth of 20 MHz. Thus, by using a multilayer structure with a single feed, dual-band operation is achieved with a reduced physical size, while still providing the necessary electrical properties. By incorporating combinatorial configuration structures, such as perturbation, truncation, and adding stubs in the design of patch antennas, circular polarization is produced by exciting the fundamental mode. This combinatorial structure explores the design space to determine the optimal configuration for a given set of design constraints without the need for a complex feed network. Thus, the structural evolution is executed while maintaining the performance requirement, and the enhancement in performance is validated through simulation. The evolved best configuration shown in Figs. 3(e) and 4(b), producing the GAGAN specifications presented in Table 2, is chosen for fabrication.

### C. ROLE OF INDIVIDUAL LAYERS

On simulating the top (Fig. 2(a)) and middle (Fig. 2(b)) layers individually with a ground plane at the bottom, the reflection coefficient and axial ratio are obtained, as depicted in Figs. 7 and 8, respectively. Upon exciting the top layer with a coax feed, a single resonance is formed at 1.15 GHz with a 10 dB impedance bandwidth of less than 20 MHz and an axial ratio of 2.2 dB to produce circular polarization (due to truncations and perturbations) at L5. Upon excitation of the middle layer containing equilateral triangular patches, resonance is obtained at 1.6 GHz with a very narrow impedance bandwidth. Moreover, the middle layer did not exhibit circular polarization in either band, because the axial ratio was greater than 6 dB in L5 and L1. By combining both layers, dual resonances at L5 and L1 are produced with 10 dB impedance bandwidth and 3 dB axial ratio bandwidth greater than 20 MHz, producing circular polarization.

**TABLE 2.** Performance comparison for structural evolution.

| Antenna | 3(a) | 3(b) | 3(c), 4(a) | 3(d), 4(a) | 3(e), 4(b) |
|---|---|---|---|---|---|
| Size($mm^3$) | 85×85×1.6 | 85×85×1.6 | 55×55×3.2 | 55×55×3.2 | 55x×55×3.2 |
| S11(dB) | L5: -19.95<br>- | L5: -22.2<br>- | L5: -17.87<br>L1: -20 | L5: -20.72<br>L1: -25.62 | L5: -26.27<br>L1: -30.62 |
| AR(dB) | L5: 22.85<br>L1: 29.79 | L5: 19.24<br>L1: 11.63 | L5: 2.71<br>L1: 15.2 | L5: 2.7<br>L1: 3.03 | L5: 1.38<br>L1: 1.64 |
| Gain(dBi) | L5: 2.71<br>L1: 2.84 | L5: 2.79<br>L1: 2.92 | L5: 2.94<br>L1: 3.15 | L5: 2.98<br>L1: 3.2 | L5: 3.18<br>L1: 3.42 |

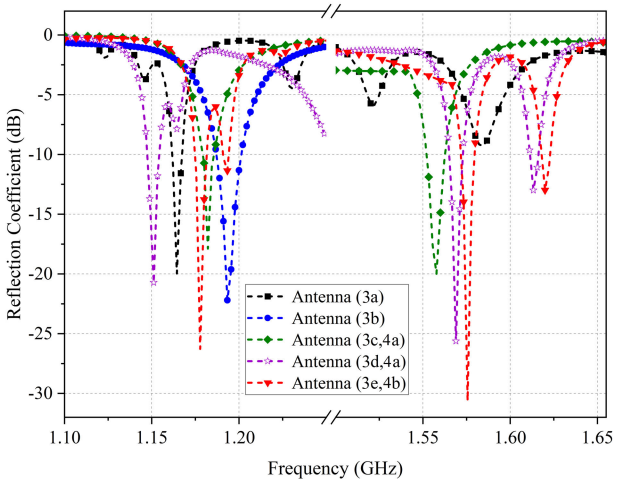


**FIGURE 5.** Reflection coefficient performance in the evolution process.

### D. FIELD DISTRIBUTION

The electric field distribution of the designed antenna is depicted in Figs. 9(a) and (b) for the two operating frequencies L5 and L1, respectively. A strong electric field

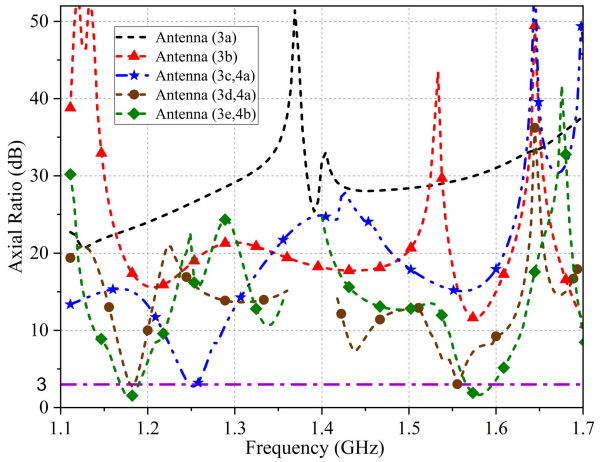


**FIGURE 6.** Axial ratio performance in the evolution process.

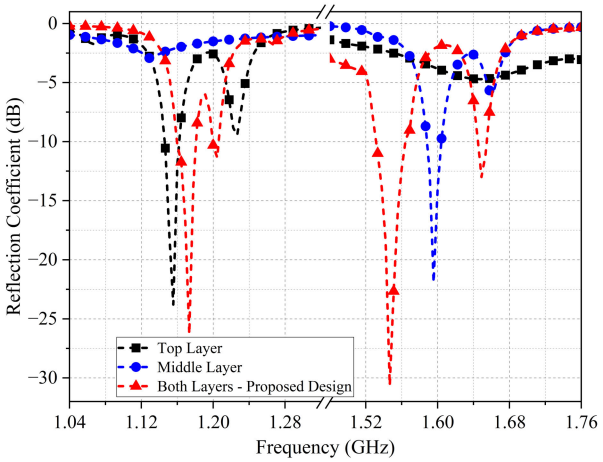


**FIGURE 7.** Reflection coefficient performance of individual layers.

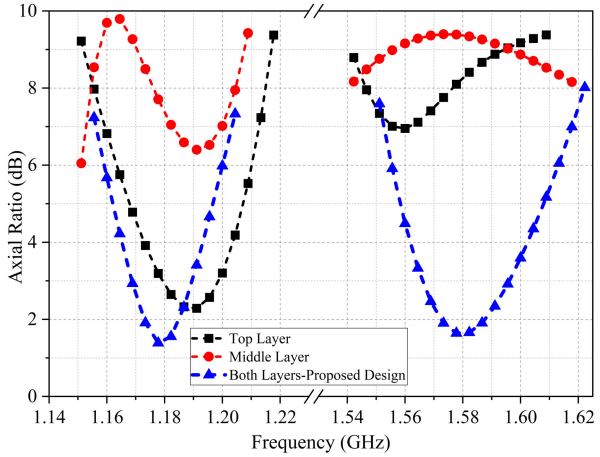


**FIGURE 8.** Axial ratio performance of individual layers.

occurs on the top layer when operated at 1.176 GHz, with a maximum distribution across the coupling gaps (d) between the resonators. When operated at 1.575 GHz, the electric fields are mostly concentrated in the middle layer producing resonance at L1. The surface current distributions of the

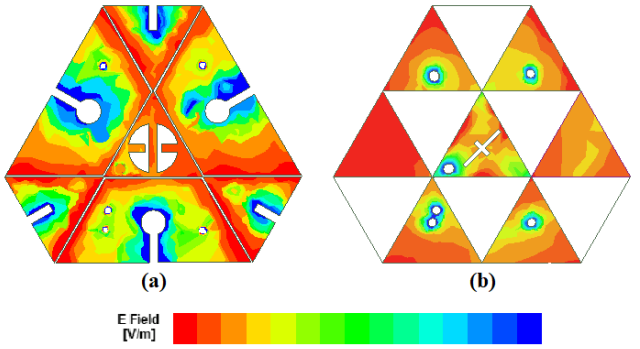


**FIGURE 9.** Electric field distribution at (a) Top layer for L5 (b) Middle Layer for L1.

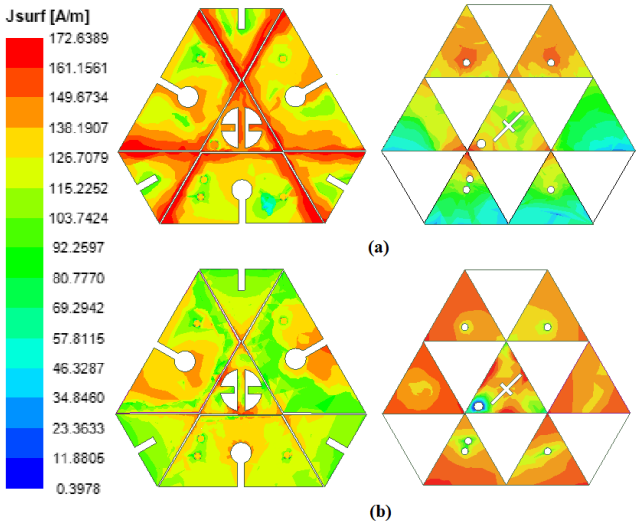


**FIGURE 10.** Surface current distribution at (a) Top layer for L5 (b) Middle Layer for L1.

proposed antenna in distinct frequency bands are shown in Fig. 10. showing a clear identification of the high surface current density (red color) for L5 and L1 with improved impedance matching. It can be observed from Fig. 10(a) that the maximum current is concentrated in the upper patch resonators loaded with slits and slots, mainly in the region around the coupling gaps, because of which the antenna exhibits frequency resonance at 1.175 GHz (L5). Furthermore, at another frequency of 1.567 GHz (L1), the current is primarily concentrated on the middle triangular patch layer and the center patch in the top layer, as shown in Fig. 10(b). Thus, as the frequency of the antenna increases, the current becomes concentrated in the middle layer, which helps to attain the improves matching at 1.156 GHz (L1). The working principle of the circularly polarized antenna is analyzed through the vector current distribution, as shown in Figs. 11 and 12 for L5 and L1, respectively, when the phases are 0°, 90°, 180°, and 270°. The perturbations and perpendicular stubs on the top layer produce two orthogonal near-degenerate modes of equal amplitude and a 90 ° phase difference at both frequencies, resulting in circular polarization (CP). In Figs. 11 and 12, the antenna surface

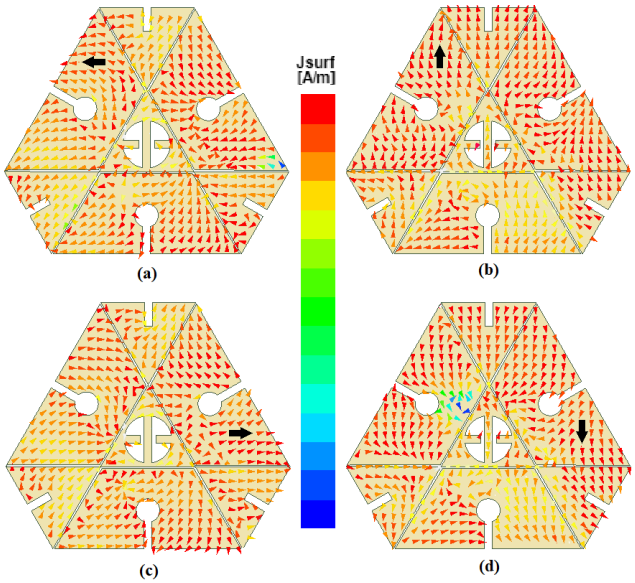


**FIGURE 11.** Vector surface current distribution at L5 for $\theta$ (a)0° (b)90° (c)180° (d)270°.

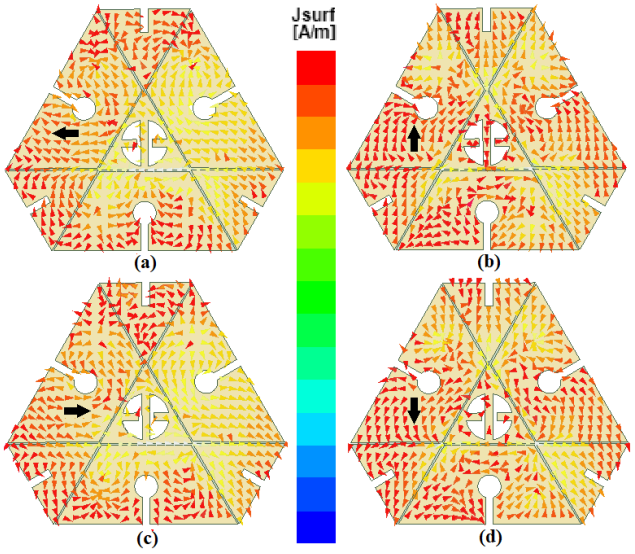


**FIGURE 12.** Vector surface current distribution at L1 for $\theta$ (a)0° (b)90° (c)180° (d)270°.

current distribution for $\theta = 0°$ and 180° is in the horizontal direction, and for $\theta = 90°$ and 270°, the vector current is in the vertical direction. Moreover, it can be observed that the rotations of the currents are clockwise; hence, left-handed CP radiation is realized for both bands. CP for both bands is confirmed by measuring the axial ratio to be less than 3 dB.

## III. PARAMETRIC ANALYSIS

The key parametric values of the designed antenna were obtained through parametric analysis. The effects of variations in the coupling gap, perturbations causing circular polarization and the effects of adding shorting pins between the patches are analyzed.

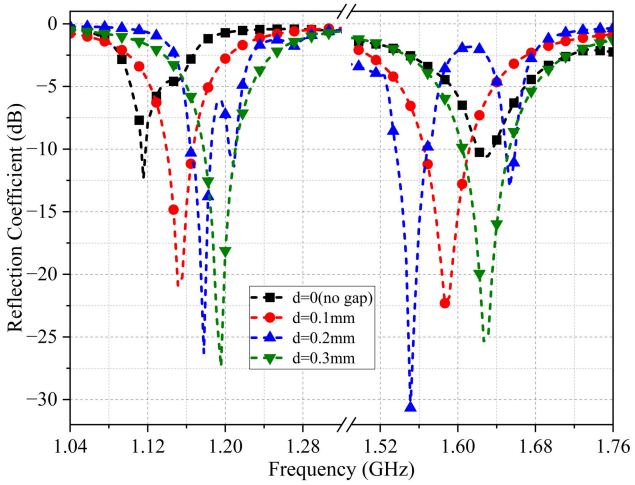


**FIGURE 13.** Effects of coupling gap (d) on reflection coefficient.

### A. EFFECTS OF COUPLING GAP ON REFLECTION COEFFICIENT

The analysis of the variations in the coupling gap (d) is shown in Fig. 13, along with the response for no coupling gap (d=0). For each incremental value of 0.1 mm, the resonance shifts towards the right. The coupling gap can be used to improve impedance matching of the antenna. The reactance of the patch element can be adjusted by adjusting the size of the coupling gap to match the impedance of the feed line better. This can increase the efficiency of the antenna and reduce the amount of power reflected. Hence it can be seen that when there is no coupling gap (d=0), the impedance matching is poor with a shift in the resonant frequency. When the gap $d$ is 0.2 mm, perfect resonance is obtained in both bands L5 and L1.

### B. EFFECTS OF PERTURBATIONS AND STUB ON AXIAL RATIO

Fig. 14(a) shows the effects of the variations in the rectangular perturbations on the axial ratio. It is observed that by decreasing the length $D_3$, the axial ratio curve in the L5 band shifts towards the left, with a value greater than 3 dB at resonance. The resonance frequencies of both bands shift from 1.176 to 1.1182 GHz and from 1.575 to 1.582 GHz as $D_3$ increases from 3 to 3.5 mm. Moreover, the axial ratio values increase from 1.38 to 4.29 dB at L5 and 1.64 to 5.91 dB at L1 affecting the circular polarization (CP) property. Thus, the perturbation $D_3$ is fixed at 3 mm to produce CP with axial ratios 1.38 and 1.64 dB at L5 and L1 respectively.

Fig. 14(b) shows the axial ratio performance owing to variations in the radius of the circular perturbations. When $R_1$ is 1.3 and 1.7 mm, the axial ratio curves shift up making the values at L5 and L1 to be greater than 3 dB resulting in a loss of polarization purity. When the radius $R_1$ is 1.5 mm, circular polarization is obtained at L5 and L1 with axial ratio values of less than 3 dB.

On adjusting the length of perpendicular stub $S_3$, the circular polarization performance can be altered as shown in Fig. 14(c). When $S_3$ is 1.44 mm, the lower resonance shifts towards the left, while the upper resonance shifts towards the right with values greater than 3 dB in both bands. When $S_3$ is 1.48 mm, both curves shift towards the right, with the L1 band having a very narrow 3 dB bandwidth. Thus, the stub length is fixed at 1.46 mm to obtain resonance at L5 and L1 with values of 1.38 and 1.64 dB respectively.

### C. EFFECTS OF SHORTING PINS ON REFLECTION COEFFICIENT AND AXIAL RATIO

The effects of the shorting pins on the reflection coefficient and axial ratio are shown in Fig. 15. Owing to the shunt inductive effect of the shorting pin, the field distribution beneath the patch becomes perturbed. Shorting pins can be used to tune the resonant frequency and control the separation between dual bands. As shown in Fig. 15(a), the shift in the reflection coefficient towards the left from the resonant frequencies can be compensated for by the addition of shorting pins. The curves are shifted towards the right from 1.14 to 1.17 GHz and 1.53 to 1.57 GHz. Moreover, there is an improvement in impedance matching owing to the introduction of shorting pins as it strengthens the field distribution.

Fig. 15(b) shows the axial ratio improvement in terms of its values and bandwidths. The axial ratio bandwidth is very narrow in the lower band, with an axial ratio of 2.7 dB at L5. With shorting pins, a bandwidth greater than 20 MHz is produced with a value of 1.38 dB. Without shorting pins, the axial ratio value in L1 is greater than 3 dB with a value of 3.03 dB, thus losing its circular polarization characteristics. Upon introducing shorting pins, the bandwidth becomes wider with an axial ratio of 1.64 dB L1.

### D. EFFECTS OF POSITION OF SHORTING PINS ON REFLECTION COEFFICIENT AND AXIAL RATIO

Based on the current distribution, we found the points of the shorting pins that provided better impedance matching. By properly positioning the shorting pins, the patch antenna performance can be optimized for the desired frequency range and application, as they adjust the resonant frequency of the patch antenna. The distance between the shorting pin and the edge of the patch affects the impedance and radiation pattern. Thus, by adding four shorting pins and varying their position of the shorting pins along the patch element, the resonant frequency can be adjusted to achieve high impedance matching and better frequency resonance. Ultimately, the position of the shorting pin(s) is optimized through simulation and/or experimentation to achieve the desired performance for the specific design and operating conditions of the antenna. The purpose and location of the shorting pins are proved experimentally and are added in Table 3, for further clarity. The preferred location is (10, 6) with high impedance matching and the best axial ratio performance. The reflection coefficient and axial ratio vary by a maximum of -5 dB and 0.15 dB respectively, on varying the position by 0.5 mm.

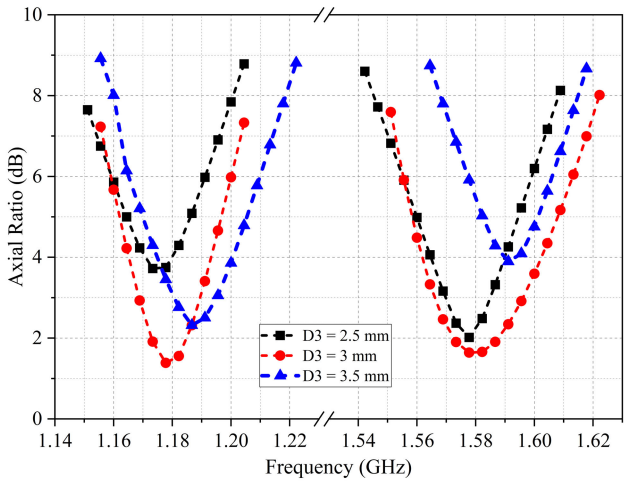


(a) Variation of rectangular perturbation $D_3$

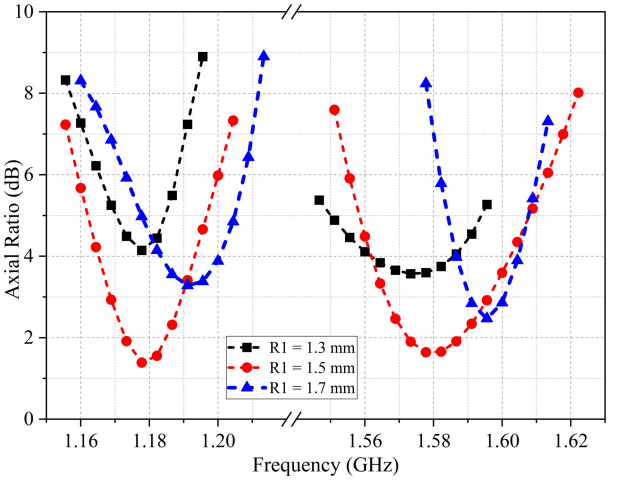


(b) Variation of dumbbell perturbation $R_1$

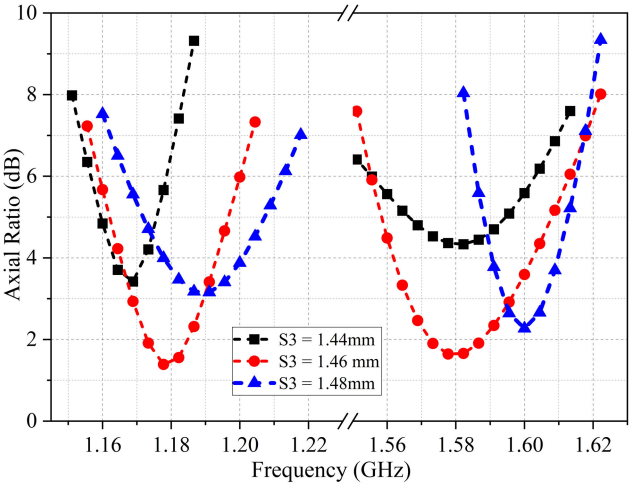


(c) Variation of perpendicular stub $S_3$

**FIGURE 14.** Effects of parametric variations on axial ratio performance.

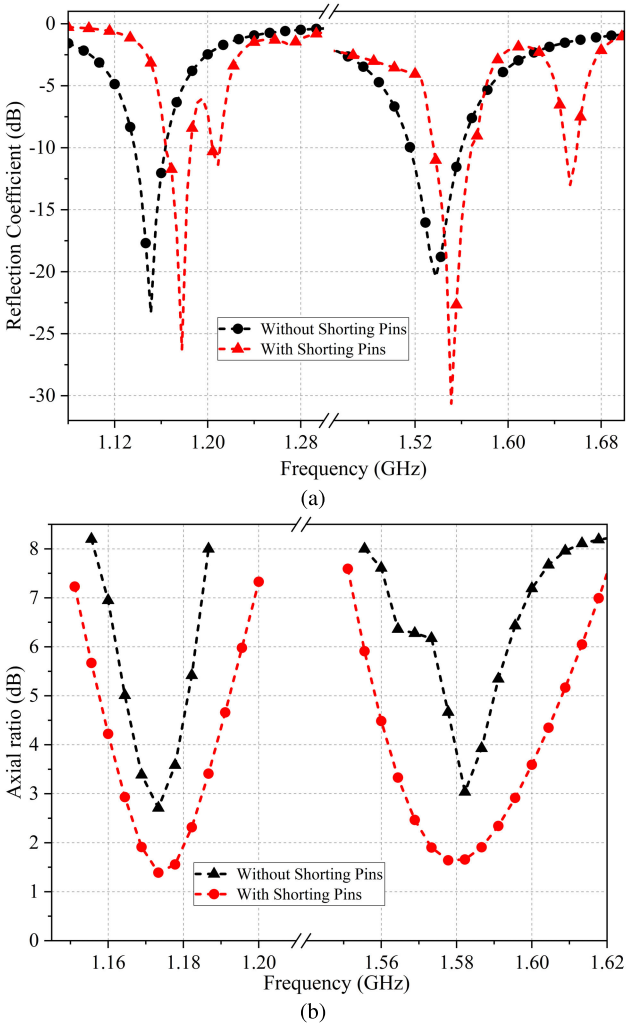


**FIGURE 15.** Effects of shorting pins on (a) Reflection coefficient (b) Axial ratio.

**TABLE 3.** Effect of position of shorting pins on reflection coefficient and axial ratio.

| Position | S11 (dB) | AR (dB) |
|---|---|---|
| **10,6** | L5: -26.27<br>L1: -30.62 | L5: 1.38<br>L1: 1.64 |
| **10,6.5** | L5: -23.05<br>L1: -25.62 | L5: 1.4<br>L1: 1.69 |
| **10,5.5** | L5: -22.93<br>L1: -26.39 | L5: 1.45<br>L1: 1.71 |
| **10.5,6** | L5: -24.53<br>L1: -25.84 | L5: 1.43<br>L1: 1.77 |
| **9.5,6** | L5: -24.98<br>L1: -27.66 | L5: 1.5<br>L1: 1.74 |

## IV. RESULTS AND ANALYSIS

### A. EXPERIMENTAL RESULTS

The design parameters of the proposed antenna are optimized to produce a compact antenna satisfying GAGAN requirements. The optimized design is fabricated as shown in Fig. 16, on a Roger RT/Duroid 6002 substrate with an overall antenna

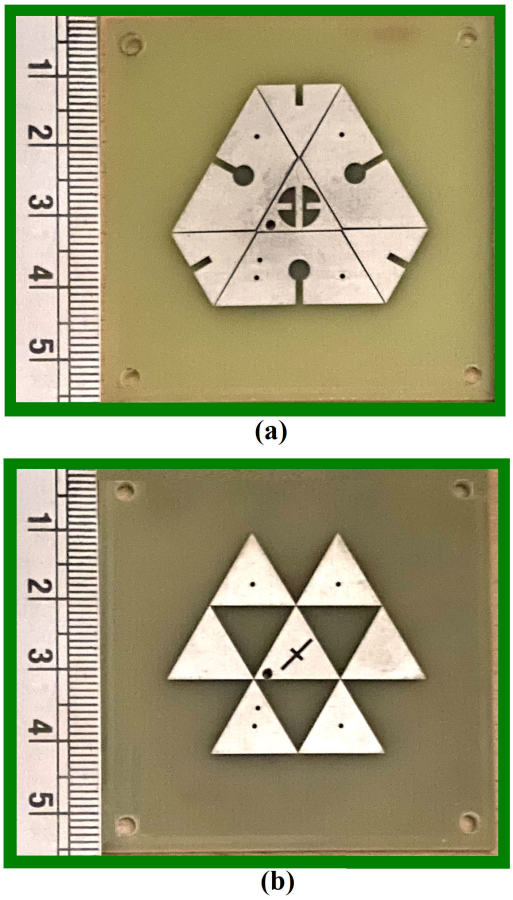


**FIGURE 16.** Fabricated antenna top view (a) Top layer (b) Middle layer.

size of 55 mm × 55 mm × 3.2 mm. The radiation patterns were measured in an anechoic chamber, where far-field measurements can be performed from 800 MHz to 8 GHz, and the reflection coefficient was measured using a Vector Network Analyzer. The simulated and measured reflection coefficient are illustrated in Fig. 17. The measured impedance bandwidth (IBW) below -10 dB is 32 MHz (1163-1195 MHz) with a 2.7% fractional bandwidth for L5 and 2.1% (1561-1595 MHz) for L1 with a 35 MHz bandwidth. The comparison between simulated and measured axial ratio (AR) curves is shown in Fig. 18, where AR bandwidth below 3 dB is 2.3% (1167-1195 MHz) with the value of 1.44 dB at L5 and 2.0% (1558-1590 MHz) with a value of 1.58 dB at L1, thus satisfying well with the GAGAN requirements. The measured response is found to be in good agreement with the simulated response. Fig. 19 shows the realized gain over the two operating frequencies. The measured peak gain at L5 and L1 are 3.41 dBi and 3.62 dBi respectively with a value greater than 3.2 dBi over the range 1.16 to 1.19 GHz and 3.5 dBi from 1.56 to 1.58 GHz throughout the bandwidth of 20 MHz. Over the entire operating band, the gain is stable with the measured gain almost equal to the simulated gain.

The simulated and measured omnidirectional radiation patterns of the proposed antenna are shown in Fig. 20 for L5. The designed hexagonal antenna radiates LHCP pattern

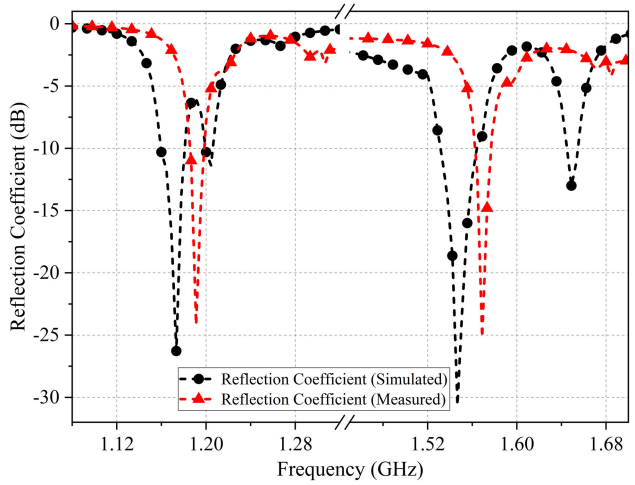


**FIGURE 17.** Reflection coefficient of the proposed antenna.

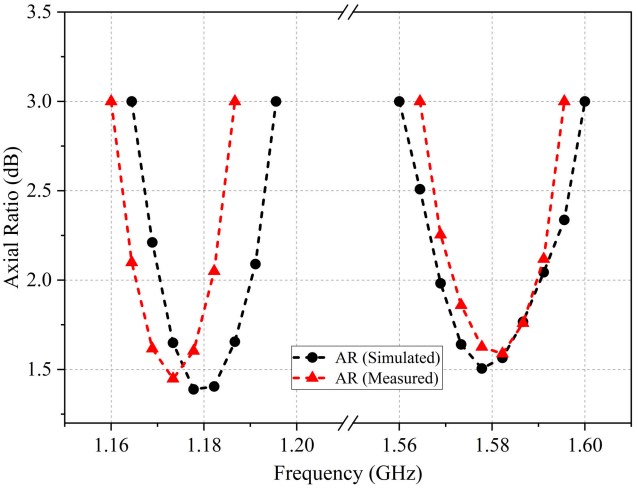


**FIGURE 18.** Axial ratio of the proposed antenna.

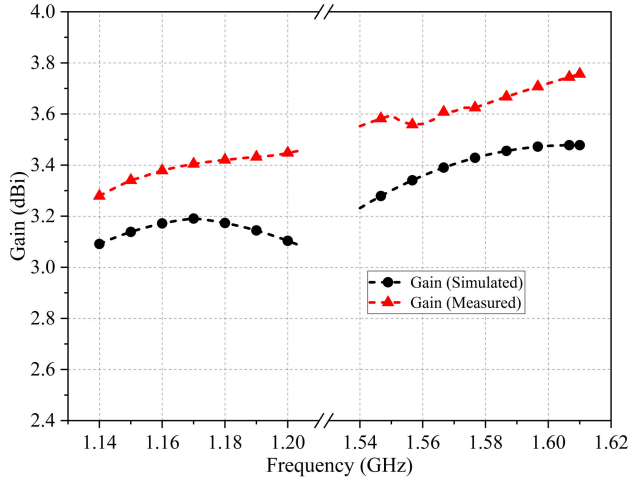


**FIGURE 19.** Gain of the proposed antenna.

having high cross-polarization levels greater than −20 dB with values −23.84 dB for $\theta = 0°$, $\phi = 0°$ and −19.63 dB

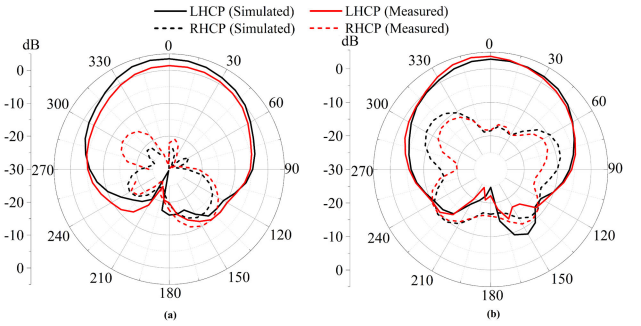


**FIGURE 20.** Radiation pattern at L5 with (a) $\theta$=0°, $\phi$=0° (b) $\theta$=0°, $\phi$=90°.

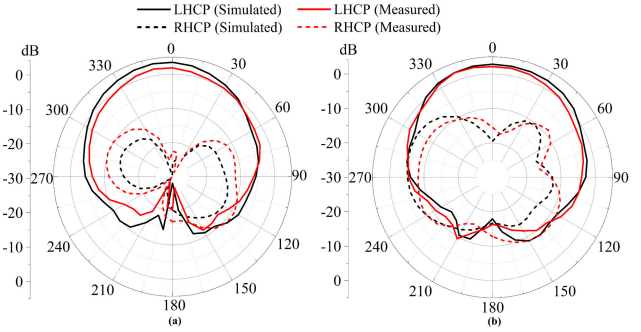


**FIGURE 21.** Radiation pattern at L1 with (a) $\theta$=0°, $\phi$=0° (b) $\theta$=0°, $\phi$=90°.

for $\theta = 0°$, $\phi = 90°$. Fig. 21, shows the realized radiation patterns at L1 with cross polarization −22.52 dB for $\theta = 0°$, $\phi = 0°$ and −18.28 dB for $\theta = 0°$, $\phi = 90°$. RHCP and LHCP radiation patterns were simulated and measured in an anechoic chamber. Owing to technical constraints, only LHCP characteristics have been reported. A comparison of the simulated and measured results is presented in Table 4 to show the deviation of the measured results from the simulated results. The imperfections due to the fabrication process, for example, slight misalignment or air gaps between the patch layers, and the precision and smoothness of the edges lead to discrepancies between the simulation and measurement results. These variations are confirmed to be within the acceptable range so as not to affect the expected GAGAN performance.

### B. PERFORMANCE COMPARISON

A performance comparison of the various antennas operating in the L-band is presented in Table 5. Although the antenna in [19] is smaller in size, it has a low gain level of less than 0.5 dBi due to a relatively smaller ground plane and is linearly polarized. In [15], [17], [20], and [23], the gain performance is higher with a wide IBW; however, the antenna is larger with a complex feed structure, making it difficult to fabricate. Although the size of the antennas in [14], [16], and [5] is large, the gain is observed to be moderate with a narrow 3 dB ARBW in [14] and [16]. The proposed antenna achieved a gain greater than 3.2 dBi despite the omnidirectional radiation characteristics that radiate energy at a wide angle, resulting in a lower gain. Hence, it is confirmed that the designed

**TABLE 4.** Simulated and measured results of the proposed hexagonal antenna.

| Parameters | $\mathbf{L}_5(S)$ | $\mathbf{L}_1(S)$ | $\mathbf{L}_5(M)$ | $\mathbf{L}_1(M)$ | $\Delta L_5(\%)$ | $\Delta L_1(\%)$ |
|---|---|---|---|---|---|---|
| Reflection Coefficient (dB) | -26.27 | -30.62 | -24.17 | -25.17 | 7.99 | 17.79 |
| 10dB IMBW (%) | 2.74 | 2.3 | 2.7 | 2.1 | 1.45 | 8.7 |
| Axial Ratio (dB) | 1.38 | 1.64 | 1.44 | 1.58 | 4.34 | 3.65 |
| 3dB ARBW (%) | 2.36 | 2.16 | 2.3 | 2.0 | 2.54 | 7.40 |
| Gain (dBi) | 3.18 | 3.42 | 3.41 | 3.62 | 7.23 | 5.84 |
| Cross Pol. (dB) | -24.82 | -25.82 | -23.84 | -22.52 | 3.94 | 12.78 |

**TABLE 5.** Performance comparison of antennas operating in L-band.

| Ref. | Size ($mm^3$) | Freq (GHz) | Feed | 10dB IBW(%) | 3dB ARBW(%) | Gain (dBi) |
|---|---|---|---|---|---|---|
| [19] | 20x20x1.6 | 1.62,2.4 | Microstrip feed line | 15.8, 6.4 | - | 0.32,0.47 |
| [12] | 50×50×3.2 | 1.176, 1.575 | Single coax feed | 1.7, 1.8 | 1.0, 1.3 | 2.52, 3.35 |
| [16] | 65×65×1.6 | 1.176, 2.332 | Single coax feed | 4, 4.2 | 1.1, 1 | 4.2, 6.6 |
| [18] | 70×45×1.6 | 1.575, 2.55, 4.5 | Microstrip feed line | 14.7, 6.8, 13.1 | 6.2, 22.7 | 2.4, 3.35, 4.5 |
| [14] | 73×73×6.4 | 1.227, 1.575 | Proximity coupled feed | 6.1, 3.7 | 1.0, 1.0 | 2.22,1.14 |
| [13] | 86×86×3.2 | 1.176, 1.575 | Single coax feed | 2.5, 2.7 | 1.5, 1.0 | 3.68, 3.31 |
| [17] | 59(radius)×1.5 | 1.207, 1.561 | Trans-directional coupler | 35.7 | 9.6, 7.1 | 1.98, 4.1 |
| [15] | 172.37×96.38×3.175 | 1.176, 1.227, 1.575 | Inset feed | 22.2, 2.4 | 11, 1.6 | 4.39, 4.19, 5.94 |
| [20] | 140×140×1.52 | 1.563 | 6-Way power divider | 11.0 | 4.8 | 5 |
| [23] | 140×140×7 | 1.288, 1.575 | 90°Hybrid coupler | 31.2 | 19.2 | 8.2 |
| This work | 55×55×3.2 | 1.176,1.575 | Singlecoax feed | 2.7, 2.1 | 2.3, 2.0 | 3.41, 3.62 |

hexagonal antenna provides a gain greater than 3.2 dBi satisfying GAGAN requirements. The proposed antenna also satisfies the required minimum impedance and axial ratio bandwidth and is found to be greater than 30 MHz. It is ascertained that the designed antenna is compact (55 mm × 55 mm) when compared to our earlier work [12], [13], with improved performance in terms of gain and bandwidth with a size reduction greater than 40%.

## V. CONCLUSION

A compact, multilayer, circularly polarized gap-coupled hexagonal microstrip antenna is designed and analyzed. The designed hexagonal antenna evolved from an equilateral triangular patch antenna as it has a smaller patch size at a given frequency than square and circular microstrip antennas. Approximately, 56.79% size reduction is achieved by using a triangular patch when compared to the conventional circular patch antenna for designing a hexagonal antenna. A compact antenna operating at L1 and L5 frequencies is obtained by incorporating combinatorial configurations, such as different geometric shapes, to achieve compactness by optimizing various parameters of the antenna while maintaining the same performance. The circuitry elements introduced in the patches excite two orthogonal near-degenerate modes that produce circular polarization (CP). A cross slot etched in the middle patch aids in gain enhancement with a value greater than 3.2 dBi throughout the 20 MHz operational bandwidth. The five shorting pins are positioned to achieve maximum impedance matching and a good CP with an axial ratio below 2 dB. The antenna produces an omnidirectional LHCP pattern with a cross-polar level greater than −22dB. The measured results are similar to the simulated results with a measured 10 dB impedance bandwidth of 2.7% (1163-1195 MHz) for L5 and 2.1% (1561-1595 MHz) for L1. The 3 dB AR bandwidth is 2.3% (1167-1195 MHz) for L5 and 2.0% (1558-1590 MHz) for L1. Thus, the proposed antenna satisfies the GAGAN requirements, making it suitable for navigation and positioning services. It has a wide range of applications, including aviation, surveying and mapping, agriculture, disaster management, maritime navigation, land transportation, and mobile communication.

## REFERENCES


[1] U R Rao Satellite Centre (URSC). *GAGAN–GPS Aided GEO Augumented Navigation*. Accessed: Nov. 20, 2022. [Online]. Available: https://www.ursc.gov.in/navigation/gagan.jsp

[2] *GPS Aided Geo Augmented Navigation (GAGAN)*. Accessed: Nov. 20, 2022. [Online]. Available: https://ijcrt.org/papers/IJCRT_197520.pdf

[3] D. M. Vijayan, M. Akhil, and S. K. Menon, "Patch loaded CPW fed monopole antenna," in *Proc. 3rd Int. Conf. Signal Process. Integr. Netw. (SPIN)*, Feb. 2016, pp. 246–249.

[4] J. Salini, S. Natarajamani, and S. M. Vaitheeswaran, "Minkowski fractal circularly polarized planar antenna for GPS application," *Proc. Comput. Sci.*, vol. 143, pp. 66–73, Jan. 2018.

[5] L. Boccia, G. Amendola, and G.-D. Massa, "A dual frequency microstrip patch antenna for high-precision GPS applications," *IEEE Antennas Wireless Propag. Lett.*, vol. 3, pp. 157–160, 2004.

[6] K. Ding, Y. Wu, K.-H. Wen, D.-L. Wu, and J.-F. Li, "A stacked patch antenna with broadband circular polarization and flat gains," *IEEE Access*, vol. 9, pp. 30275–30282, 2021.

[7] T.-Y. Han and C.-Y.-D. Sim, "Shorted planar triangular patch antenna with dual-frequency operation," *AEU-Int. J. Electron. Commun.*, vol. 63, no. 2, pp. 103–107, Feb. 2009.

[8] R. K. Choudhary, J. K. Mandal, and D. Bhattacharyya, *Advanced Computing and Communication Technologies*. Singapore: Springer, 2018.

[9] S. Dasgupta, B. Gupta, and H. Saha, "Compact equilateral triangular patch antenna with slot loading," *Microw. Opt. Technol. Lett.*, vol. 56, no. 2, pp. 268–274, Feb. 2014.

[10] J. P. Wang, Q. W. Liu, and L. Zhu, "Bandwidth enhancement of a differential-fed equilateral triangular patch antenna via loading of shorting posts," *IEEE Trans. Antennas Propag.*, vol. 65, no. 1, pp. 36–43, Jan. 2017.
[11] B. Chinnagurusamy, M. Perumalsamy, and A. S. Thankamony Sarasam, "Design and fabrication of compact triangular multiband microstrip patch antenna for C- and X-band applications," *Int. J. Commun. Syst.*, vol. 34, no. 15, p. e4939, 2021.
[12] C. Sahana, N. M. Devi, and M. Jayakumar, "Multilayer pentagon ring dual-band microstrip antenna for GPS aided GEO augmented navigation receivers," in *Proc. IEEE Region 10 Symp. (TENSYMP)*, Jul. 2022, pp. 1–4, doi: 10.1109/TENSYMP54529.2022.9864445.
[13] C. Sahana and M. Jayakumar, "Dual-band circularly polarized annular ring patch antenna for GPS-aided GEO-augmented navigation receivers," *IEEE Antennas Wireless Propag. Lett.*, vol. 21, no. 9, pp. 1737–1741, Sep. 2022.
[14] N. Pham, J.-Y. Chung, and B. Lee, "A proximity-fed antenna for dual-band GPS receiver," *Prog. Electromagn. Res. C*, vol. 61, pp. 1–8, 2016.
[15] S. Mishra, S. Das, S. S. Pattnaik, S. Kumar, and B. K. Kanaujia, "Low-profile circularly polarized planar antenna for GPS L1, L2, and L5 bands," *Microw. Opt. Technol. Lett.*, vol. 62, no. 2, pp. 806–815, 2019.
[16] S. D. Choudhary, A. Srivastava, and M. Kumar, "Design of single-fed dual-polarized dual-band slotted patch antenna for GPS and SDARS applications," *Microw. Opt. Technol. Lett.*, vol. 63, no. 1, pp. 353–360, 2021.
[17] H. Liu, C. Xun, S.-J. Fang, and Z. Wang, "Compact dual-band circularly polarized patch antenna with wide 3-DB axial ratio beamwidth for beidou applications," *Prog. Electromagn. Res. M*, vol. 87, pp. 103–113, 2019.
[18] M. A. Al-Mihrab, A. J. Salim, and J. K. Ali, "A compact multiband printed monopole antenna with hybrid polarization radiation for GPS, LTE, and satellite applications," *IEEE Access*, vol. 8, pp. 110371–110380, 2020.
[19] R. S. Daniel, R. Pandeeswari, and S. Raghavan, "A miniaturized printed monopole antenna loaded with hexagonal complementary split ring resonators for multiband operations," *Int. J. RF Microw. Comput.-Aided Eng.*, vol. 28, no. 7, Sep. 2018, Art. no. e21401.
[20] H. Liao and A. Shamim, "A low-profile and high-aperture-efficiency hexagonal circularly polarized microstrip antenna array," *IEEE Antennas Wireless Propag. Lett.*, vol. 21, no. 3, pp. 615–619, Mar. 2022.
[21] S.-W. Zhou, P.-H. Li, Y. Wang, W.-H. Feng, and Z.-Q. Liu, "A CPW-fed broadband circularly polarized regular-hexagonal slot antenna with L-shape monopole," *IEEE Antennas Wireless Propag. Lett.*, vol. 10, pp. 1182–1185, 2011.
[22] Y. Ha, J.-I. Jung, S. Lee, and S. Pyo, "Extremely low-profile monopolar microstrip antenna with wide bandwidth," *Sensors*, vol. 21, no. 16, p. 5295, Aug. 2021.
[23] K. Ding, T. Yu, and Q. Zhang, "A compact stacked circularly polarized annular-ring microstrip antenna for GPS applications," *Prog. Electromagn. Res. Lett.*, vol. 40, pp. 171–179, 2013.
[24] P. S. Hall and J. R. James, *Handbook of Microstrip Antennas*. London, U.K.: Institution of Electrical Engineers, 1989.
[25] K. Qian and X. Tang, "Compact LTCC dual-band circularly polarized perturbed hexagonal microstrip antenna," *IEEE Antennas Wireless Propag. Lett.*, vol. 10, pp. 1212–1215, 2011.

**C. SAHANA** (Graduate Student Member, IEEE) received the bachelor's degree in electronics and communication engineering (ECE) from the PSG College of Technology, India, in 2014, and the M.E. degree from Amrita Vishwa Vidyapeetham, Ettimadai, India, in 2017. She is currently a Research Scholar with Amrita Vishwa Vidyapeetham. Her research interest includes microstrip antennas in space applications.

**M. NIRMALA DEVI** (Member, IEEE) received the B.E. degree in electronics and communication engineering (ECE) from the Government College of Technology, Coimbatore, in 1990, the M.E. degree in applied electronics from Bharathiyar University, in 1996, and the Ph.D. degree in VLSI design of artificial neural networks from Anna University, Chennai, in 2010. She is currently a Professor with the Amrita School of Engineering, Amrita Vishwa Vidyapeetham, Coimbatore. Her research interests include VLSI design and testing, computational intelligence, hardware security and trust, evolvable 997 hardware, and RF CMOS system design.

**M. JAYAKUMAR** (Member, IEEE) received the Ph.D. degree in microwave devices from the University of Delhi, in 1996. He is currently a Professor with the Department of Electronics and Communication Engineering, Amrita Vishwa Vidyapeetham University, Coimbatore. He has published more than 90 research papers in journals and conferences. His research interests include specialized antennas and RF systems for space and defense applications. Most of his research works involve compact conformal antennas for air-borne vehicle communication, specialized unconventional materials for RF absorbers, and compact antenna systems for 5G and beyond.